

Short Communication

Theoretical Study of Oxygen Adsorption on a Metal (Ni, Rh, Pd, Pt)-Doped Au(111) Surface

Mei Xue^{1,2}, Jianfeng Jia¹, Haishun Wu^{1,*}

¹ School of Chemistry and Materials Science, Shanxi Normal University, Linfen, 041004,

² Graduate School, Taiyuan University of Science and Technology, Taiyuan, 030024,

*E-mail: 2021032@tyust.edu.cn

Received: 14 March 2022 / Accepted: 4 May 2022 / Published: 6 June 2022

Elucidating the doping of transition metals with different structural units on the catalyst surface is very important for improving the catalytic performance of heterogeneous catalysts. In this work, the adsorption performance of O₂ molecules on the surface of bimetallic catalysts doped with different structural units was investigated using a density functional theory (DFT) method. The effects of different structural units on O₂ adsorption are clarified. It is concluded that among the four transition metal-doped bimetallic catalysts, when TM=Ni, the performance of O₂ adsorption is stronger than that of the other three metal-doped gold-based bimetallic catalysts. When the doped structure is a dimer, the adsorption energy after O₂ adsorption is greater than monomer and trimer doping. However, the bond length and the number of transferred electrons are lower than those after trimer doping.

Keywords: Adsorption; Bimetallic catalysts; DFT; Structural unit

1. INTRODUCTION

In the field of heterogeneous catalysis, research on the surface structure and composition of solid material particles is a current hotspot[1]. Exploring the surface structure can improve the selectivity and catalytic activity of heterogeneous catalysts more efficiently[2-4]. Bimetallic catalysts often have significantly different physical and chemical properties than their parent metal due to their unique composition, making them an important heterogeneous catalyst[5-11]. Since 1987, Haruta et al. have made breakthroughs in the research of nanogold catalysts, and Au has attracted the attention of researchers as a catalyst[12]. Although the Au catalyst exhibits a certain catalytic activity, there are still limitations in the actual application process. To improve its catalytic activity and reuse rate[12-14], a common method at this stage is to dope a second metal on its surface[16-19]. In current gold-based bimetallic catalysts, most doping metals used are transition metals[20-27].

O₂ molecules are essential reactants in many chemical reactions and can act as oxidants. Activation of molecular oxygen is a critical step in many heterogeneous oxidation processes, including electrocatalysis[28-31]. With the increasingly serious energy crisis, the research on new energy materials has become very urgent, among which methanol fuel cells and their oxidation electrocatalysts are the focus of research[29,32-35]. Many transition metal gold-based bimetallic catalysts participating in catalyzed chemical reactions involve the participation of oxygen molecules[36-43], such as the oxidation of CO, the selective oxidation of alcohols, and the preparation of water. The activation of molecular O₂ is also a key step in the aerobic oxidation reaction on Au-based catalysts. The activation of oxygen is still a bottleneck in the entire catalytic process. Therefore, the adsorption and activation of oxygen molecules on the catalyst surface is an critical part of exploring the catalytic mechanism of gold-based bimetallic catalysts[44-47]. Pinto et al. studied the adsorption and decomposition of oxygen on the surface of PdPt/Au(111) by density functional theory and concluded that the Fcc site on the surface of the alloy is most conducive to the combination of O₂ and the surface[48]. Chang et al. used DFT theory to study the process of selective oxidation of formaldehyde to methanol by O₂ molecules on the surface of Pd-Au bimetallic catalysts with different surface structural units[49]. The study showed that the presence of Pd significantly improved the adsorption and activation of O₂ on the alloy surface. Studying the unit structure on the surface of the bimetallic catalyst is necessary to understand the catalytic performance.

Currently, DFT is an integral method for conducting theoretical research on multi-electron systems[49-53]. The purpose of this article is to use a DFT calculation to study the adsorption of O₂ molecules on a transition metal (TM=Ni, Rh, Pd, Pt)-doped Au(111). We investigated various possible adsorption sites of oxygen molecules on the surface of gold-based bimetallic catalysts, conducted further structural and energy analyses on these stable adsorption configurations, and finally completed Bader charge analysis. We believe that this work has certain guiding significance for the rational design of heterogeneous catalysts for dissociation reactions.

2. METHODS AND MODELS

The calculation software used in this paper is the Vienna Ab-initio Software Package(VASP) package, which the electron-ion interaction uses the projected enhanced wave (PAW) method, and the generalized gradient approximation (GGA) of Perdew-Burke-Ernzerhof (PBE) is used to represent the exchange correlation function. The surface Brillouin zone uses a (5×5×1) k-point mesh and selects a plane wave cutoff energy of 400 eV. The convergence conditions of the structure is when the force change is less than 0.02 eV·Å⁻¹ and the energy difference is less than 1×10⁻⁴ eV.

O₂ molecules were adsorbed on the constructed TM_{single}-Au(111), TM_{dimer}-Au(111), TM_{trimer}-Au(111)(TM=Ni, Rh, Pd, Pt) gold base bimetal surfaces, and various possible adsorption sites were simulated, this can refer to our previous work[54], as shown in Figure 1. After optimizing the structure, the most stable adsorption configuration was obtained and the adsorption energy was calculated. After the structure optimization, the most stable adsorption configuration was obtained and

the adsorption energy (E_{ads}) was calculated. The adsorption energy was calculated according to the following formula:

$$E_{\text{ads}} = E_{\text{slab/adsorbate}} - E_{\text{slab}} - E_{\text{adsorbate}} \quad (1)$$

Where $E_{\text{slab/adsorbate}}$ is the total energy of the catalyst surface after adsorbing O_2 , E_{slab} is the total energy of Au(111) on the pure surface, and $E_{\text{adsorbate}}$ is the energy of a single oxygen molecule.

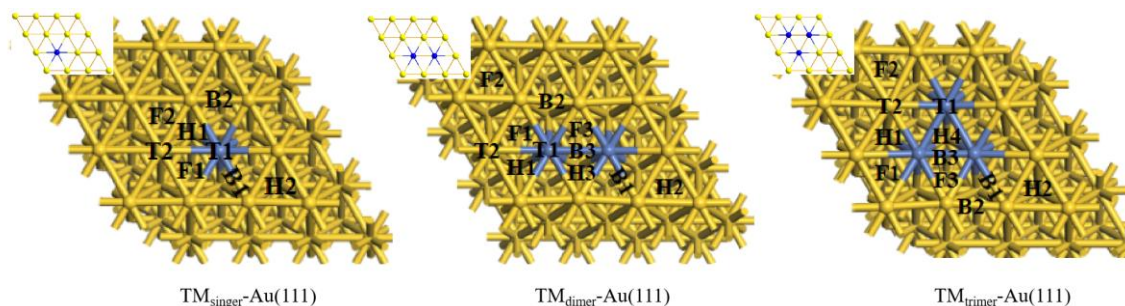


Figure 1. Surface structure and possible doping sites of gold based bimetallic catalysts with different doping structure units. Au atoms are shown in yellow; the doped metals are indicated in blue[54]

3. RESULTS AND DISCUSSION

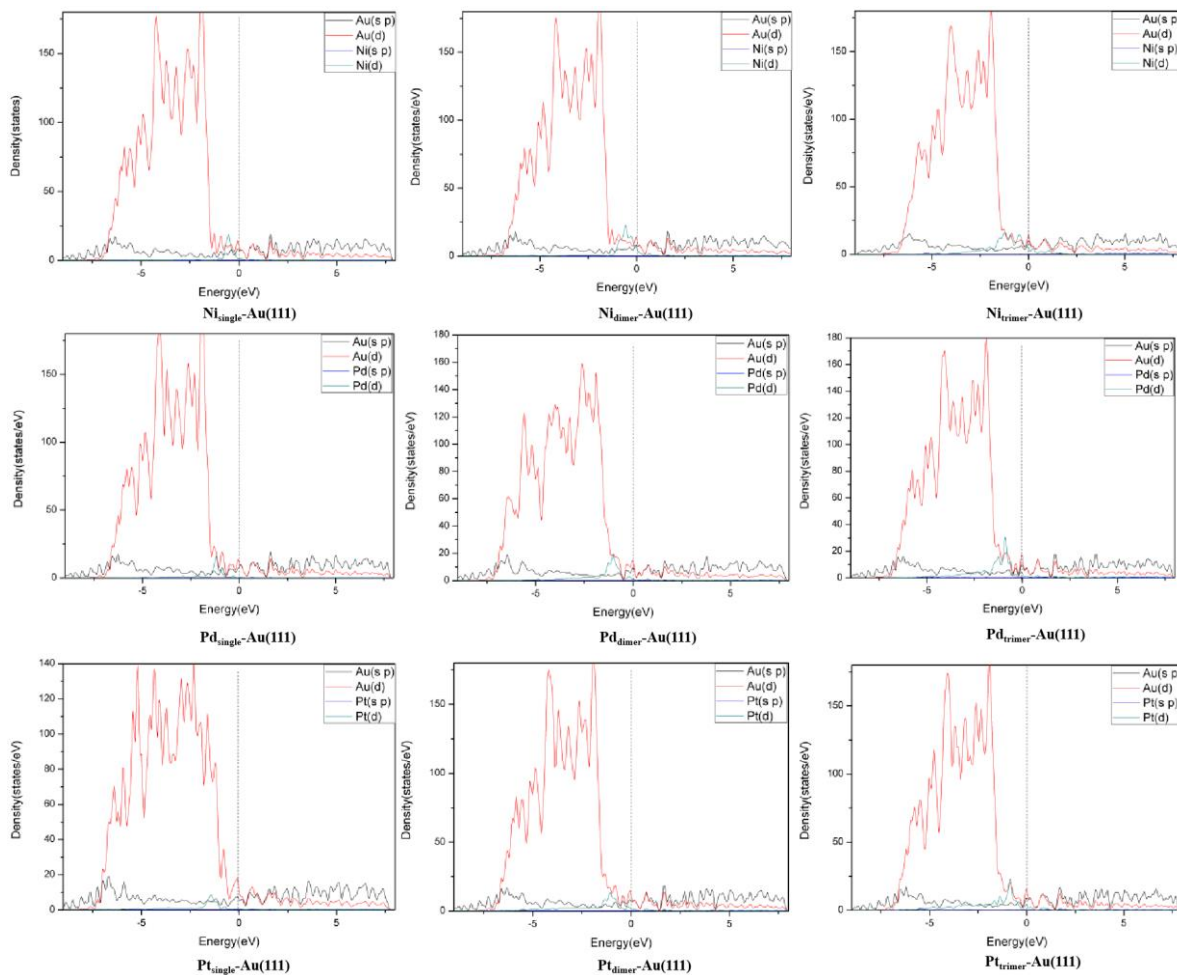
3.1 TM-Au(111) bimetallic structural analysis and charge analyses

The distance between Au and Au on the pure surface of Au(111) is 2.938 Å. When the surface is doped with transition metals (TM=Ni, Rh, Pd, Pt) of different structural units, the distance between TM-Au decreases, but the change is not significant. On the Ni-doped Au(111) surfaces, the distance between Ni-Au changes the most compared with the original Au-Au distance. The distance between Pd-Au on the Pd-doped Au(111) surfaces has the smallest change compared with the initial Au-Au distance, as shown in Table. 1.

According to the state density diagram analysis, as shown in Figure 2, the surface of TM-Au(111) exhibits metal properties. There is a certain electron region near the Fermi level (energy is zero), indicating that TM-Au(111) has good electron conductivity, and there is orbital hybridization between TM and Au near the Fermi level. On the Ni-Au(111) bimetallic surface, DOS is mainly the hybridization of the Au and Ni d orbitals for the part just below the Fermi level. While for the part just above the Fermi level, DOS is mainly the hybridization of the Au sp and d orbitals. However, when the TM is Pd, Pt, or Rh and doped in the form of a monomer, the part just below the Fermi level is mainly the Au d orbital contribution, and the Au sp orbital also has a small contribution. Just above the Fermi level, DOS is mainly a hybridization of Au sp and d orbitals. When doped in the form of dimers and trimers, DOS is mainly a hybridization of Au sp and d orbitals just below the Fermi level, while Pd d orbitals also contribute. For the part just above the Fermi level, DOS is mainly a hybridization of Au sp and d orbitals, with a small Pd d orbital contribution. By increasing the number of doping metals, the contribution of the TM d orbital is enhanced, and the interaction with Au is also increased.

Table 1. Distance between TM-Au and Bader charge analysis of different structural units of TM-Au(111)(TM=Ni, Rh, Pd, Pt) bimetals

TM	Parameters	TM _{single} -Au	TM _{dimer} -Au	TM _{trimer} -Au
Ni	Ni-Au distance (Å)	2.876	2.833	2.869
	Bader charge/Ni (e)	0.33	0.32	0.27
Pd	Pd-Au distance (Å)	2.923	2.916	2.904
	Bader charge/Pd (e)	0.06	0.06	0.04
Pt	Pt-Au distance (Å)	2.908	2.904	2.880
	Bader charge/Pt (e)	-0.12	-0.11	-0.09
Rh	Rh-Au distance (Å)	2.892	2.912	2.932
	Bader charge/Rh (e)	0.13	0.13	0.11



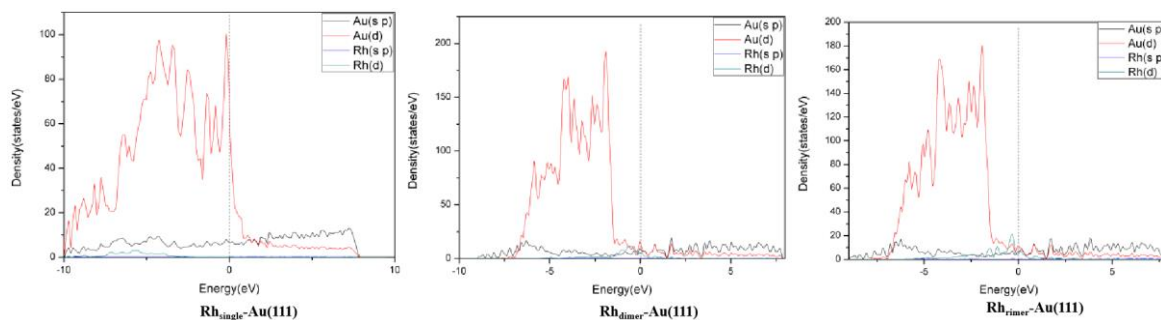


Figure 2. Density diagram of DOS states on the TM-Au (111)(TM =Ni, Rh, Pd, Pt) bimetal surfaces

To better analyze the surface charge transfer of the TM-Au(111) bimetal, we carried out Bader charge analysis for these gold-based bimetal catalysts with different structural units. Bader charge analysis can quantitatively calculate the charge transfer of surface atoms. In general, the more electronegative an element is, the easier it is to gain electrons. In contrast, the less electronegative an element is, the easier it is to lose electrons. Therefore, the charge is transferred from less electronegative elements to more electronegative elements. According to Pauling, the electronegativity of Au is 2.40, Ni 1.91, Rh 2.28, Pd 2.20, and Pt 2.20. As seen in Table 1, the electron transfer direction on the TM-Au(111)(TM=Ni, Rh, Pd, Pt) bimetal surface is from the transition metal (TM=Ni, Rh, Pd, Pt) to the Au atom. The exception is for Pt_{trimer}-Au(111) bimetallic surfaces. The transfer of charge between atoms depends not only on electronegativity but also on the distance between atoms. The distance between Pd-Au and Au-Au in the Pd-Au(111) bimetallic catalyst is the smallest. There is little difference in electronegativity, so there is almost no charge transfer.

3.2 Energy analysis and structural analyses of O₂ molecule adsorption

In order to better describe the different adsorption sites on the gold-based bimetallic surface, in this paper, T1(Top_{TM}) and T2(Top_{Au}) are used to represent two top adsorption sites, B1(Bridge_{TM-Au}), B2(Bridge_{Au-Au}), and B3(Bridge_{TM-TM}) are used to represent three bridge adsorption sites, and H1(Hcp_{Au-TM-Au}), H2(Hcp_{Au-Au-Au}), H3(Hcp_{TM-Au-TM}), and H4(Hcp_{TM-TM-TM}) are used in this paper. Four Hcp sites are represented, and F1(Fcc_{Au-TM-Au}), F2(Fcc_{Au-Au-Au}), F3(Fcc_{TM-Au-TM}), and F4(Fcc_{TM-TM-TM}) are used to represent four Fcc sites, as shown in Figure 1. The stable adsorption configuration and corresponding adsorption energy are described below.

As shown in Figure 3 and Table 2, the stable adsorption of O₂ molecules on the surface of Ni_{single}-Au(111) occurs at the F1 site; the stable adsorption of O₂ molecules on the surfaces of Pd_{single}-Au(111), Pt_{single}-Au(111), and Rh_{single}-Au(111) occurs at the H1 site. Our calculations indicate that O₂ molecules preferably adsorb on TM sites of mentioned TM-Au surfaces, which consistent with previous theoretical studies[55-58]. When O₂ molecules are adsorbed on the surfaces of TM_{single}-Au(111)(TM=Ni, Rh, Pd, Pt) bimetal in a stable configuration, the adsorption energies are -78.15, -33.77, -10.16, and -40.52 kJ/mol, respectively. The stable adsorption of O₂ molecules on the surface of TM_{dimer}-Au(111)(TM=Ni, Rh, Pd, Pt) bimetal are all at the B3 site. When O₂ molecules are adsorbed on the surfaces of the TM_{dimer}-Au(111)(TM=Ni, Rh, Pd, Pt) bimetal in a stable configuration,

the adsorption energies are -189.11, -205.51, -66.57, and -85.87 kJ/mol, respectively. The stable structures of the Ni_{trimer}-Au(111), Pd_{trimer}-Au(111), and Pt_{trimer}-Au(111) gold-based bimetallic surfaces doped with O₂ molecules in the trimeric structural unit are all O₂ molecules adsorbed on the F4 position. Only on the surface of Rh_{trimer}-Au(111) is the O₂ molecule adsorbed on the bridge position of Rh-Rh, which is the B3 position. When O₂ molecules are adsorbed on the surfaces of TM_{trimer}-Au(111) (TM=Ni, Rh, Pd, Pt) bimetal in a stable configuration, the adsorption energies are -180.43, -183.32, -75.26, and -59.82 kJ/mol, respectively. Compared with surface of pure gold [59,60], the addition of the second metal increase the adsorption energy of O₂ molecule, which is consistent with the result on Pd-Au(111)[49].

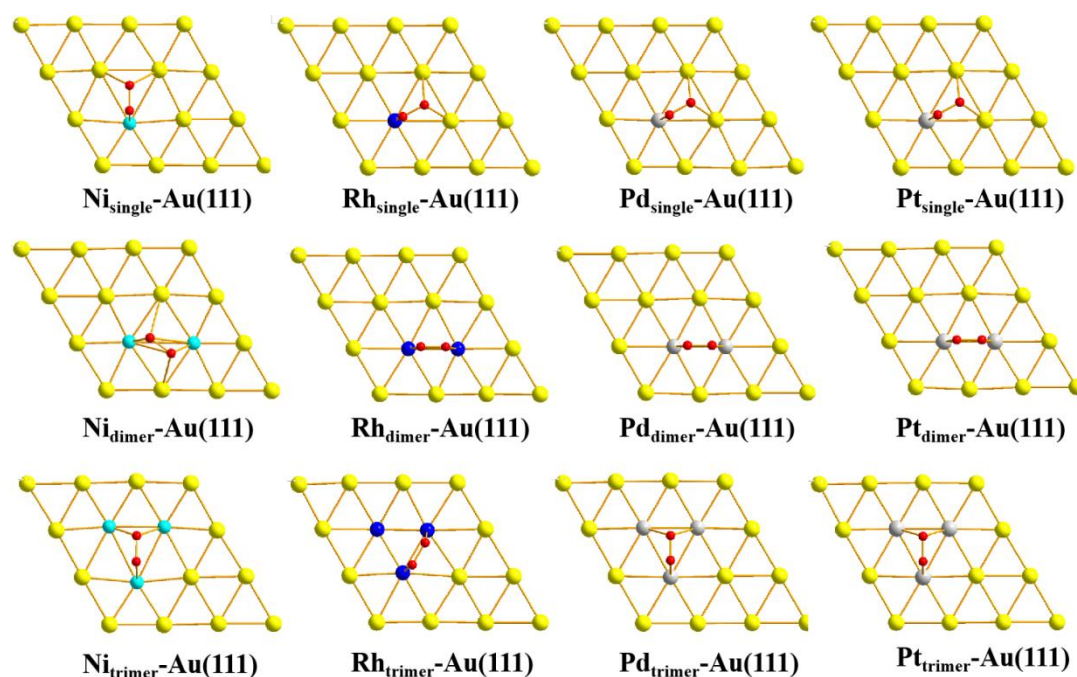


Figure 3. Adsorption configurations of O₂ molecular on the TM_{single}-Au(111), TM_{dimer}-Au(111) and TM_{trimer}-Au(111)(TM=Ni, Rh, Pd, Pt) surfaces

Table 2 shows that when the O₂ molecule is in the stable adsorption structure on the surface of TM_{single}-Au(111)(TM=Ni, Rh, Pd, Pt), the distances between O-O are 1.383, 1.334, 1.341 and 1.359 Å, respectively. On the surface of TM_{dimer}-Au(111)(TM=Ni, Rh, Pd, Pt) with stable O₂ adsorption, the O-O distances are 1.413, 1.370, 1.336 and 1.374 Å, respectively. On the surface of TM_{trimer}-Au(111) (TM=Ni, Rh, Pd, Pt) with stable O₂ adsorption, the distances between O-O are 1.455, 1.373, 1.369 and 1.412 Å, respectively. The distance of O-O in gas is 1.24 Å. The comparison shows that after O₂ molecules are adsorbed on the surfaces of TM-Au(111)(TM=Ni, Rh, Pd, Pt), the bond length between O-O becomes larger, which is close to peroxide O₂²⁻ (O-O bond length: 1.30-1.55 Å[61]). Similarly, the O-O bond lengths of Pd-Au(111) surface were 1.31-1.35 Å[49].

Table 2. The bond length, adsorption energy, and Bader charge of O₂ molecules adsorbed on the surface of TM-Au(111) with different structural units

TM	Parameters	single atom	dimer atoms	trimer atoms
Ni	O-O distance (Å)	1.383	1.413	1.455
	Ni-O distance (Å)	1.803	1.831	1.857
	E_{ads} (kJ/mol)	-78.15	-189.11	-180.43
	Bader charge/Ni (e)	0.54	0.51	0.47
	Bader charge/O ₂ (e)	-0.68	-0.77	-0.80
Rh	O-O distance (Å)	1.334	1.370	1.373
	Rh-O distance (Å)	1.904	1.928	1.929
	E_{ads} (kJ/mol)	-33.77	-205.51	-183.32
	Bader charge/Rh (e)	0.37	0.35	0.28
	Bader charge/O ₂ (e)	-0.48	-0.52	-0.53
Pd	O-O distance (Å)	1.341	1.336	1.369
	Pd-O distance (Å)	2.025	2.045	2.135
	E_{ads} (kJ/mol)	-10.61	-66.57	-75.26
	Bader charge/Pd (e)	0.28	0.26	0.23
	Bader charge/O ₂ (e)	-0.53	-0.46	-0.59
Pt	O-O distance (Å)	1.359	1.374	1.412
	Pt-O distance (Å)	2.007	2.027	2.137
	E_{ads} (kJ/mol)	-40.52	-85.87	-59.82
	Bader charge/Pt (e)	0.16	0.15	0.11
	Bader charge/O ₂ (e)	-0.57	-0.52	-0.64

3.3 State density analysis on O₂ molecule adsorption

Compared with the DOS of the Ni-Au monomer before and after oxygen adsorption, as shown in Figure 4, it can be seen that the DOS of the Ni-Au monomer just above the Fermi level basically does not change. However, for DOS just below the Fermi level, the contribution of the Ni d orbital is obviously weakened. The decreasing part mainly corresponds to the contribution of the O sp orbital, indicating a strong interaction between O and Ni. Similarly, by comparing the DOS of Pd-Au, Pt-Au and Rh-Au monomers before and after oxygen adsorption, it can be seen that the DOS just above the Fermi level basically do not change. However, for DOS just below the Fermi level, the contribution of the Au d orbital is obviously weakened. The decreasing part mainly corresponds to the contribution of the O sp orbital, indicating a strong interaction between O and Au. Similarly, by comparing the DOS of Pt-Au and Rh-Au monomers before and after oxygen adsorption, it can be seen that the DOS of Pt-Au and Rh-Au monomers just above the Fermi level basically do not change. However, for DOS just

below the Fermi level, the contribution of the Au d orbital is obviously weakened. The decreasing part mainly corresponds to the contribution of the O sp orbital, indicating a strong interaction between O and Au.

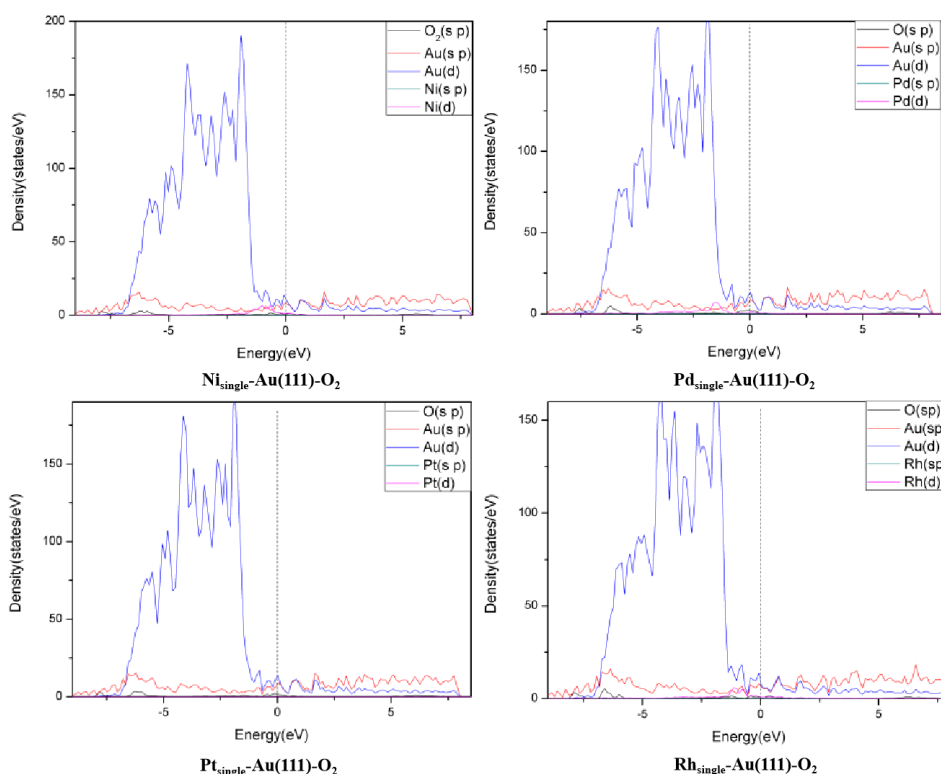


Figure 4. DOS diagram of the $\text{TM}_{\text{single}}\text{-Au}(111)$ ($\text{TM}=\text{Ni}, \text{Rh}, \text{Pd}, \text{Pt}$) bimetal surface-adsorbed O_2 molecule stable configuration

By comparing the DOS of the Ni-Au dimer before and after oxygen adsorption, as shown in Figure 5, it can be seen that the DOS of the Ni-Au dimer greater than and near the Fermi level basically does not change. However, for DOS smaller than and near the Fermi level, the contribution of Ni d and Au d orbitals is obviously weakened. The decreasing part mainly corresponds to the contribution of the O sp orbital, indicating a strong interaction between O and Ni and Au. Similarly, the comparison of DOS before and after oxygen adsorption by Pd-Au, Pt-Au and Rh-Au dimers shows that the variation rule is the same as that of Ni, indicating that there is a strong interaction between O, Au and TM.

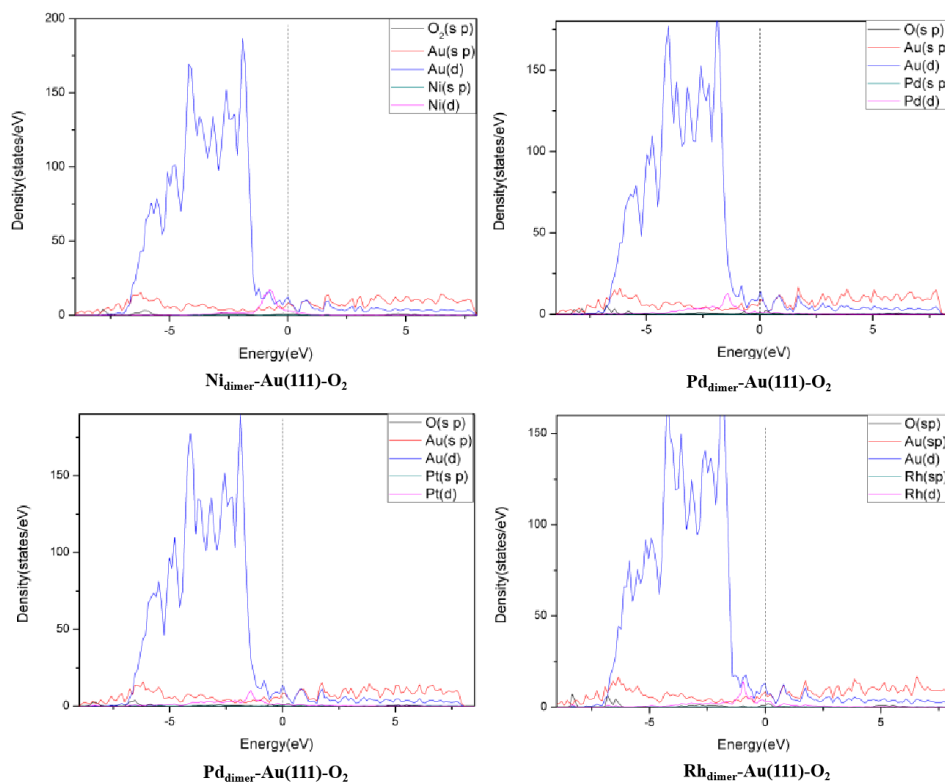


Figure 5. DOS diagram of the $TM_{dimer}\text{-Au(111)-O}_2$ (TM=Ni, Rh, Pd, Pt) bimetal surface-adsorbed O_2 molecule stable configuration

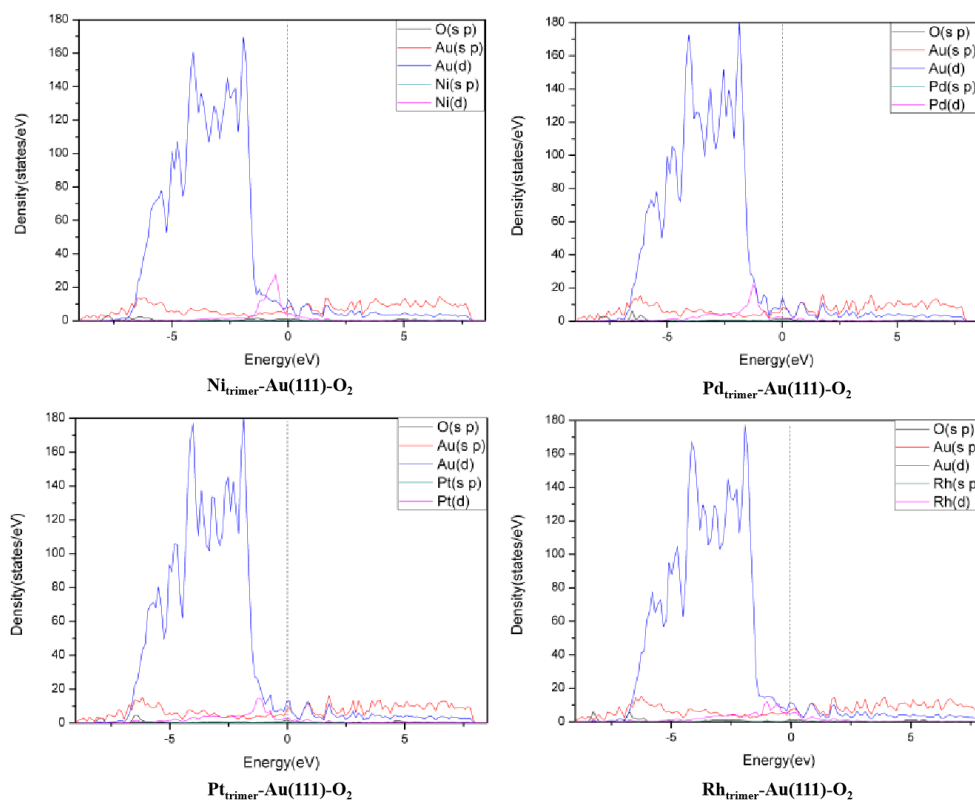


Figure 6. DOS diagram of the $TM_{trimer}\text{-Au(111)-O}_2$ (TM=Ni, Rh, Pd, Pt) bimetal surface-adsorbed O_2 molecule stable configuration

Compared with the DOS of the Ni-Au trimer before and after oxygen adsorption, as shown in Figure 6, the DOS of the Ni-Au trimer just above the Fermi level basically does not change. However, for DOS just below the Fermi level, the contributions of the Ni d and Au sp and d orbitals are obviously weakened. The decreasing part mainly corresponds to the contribution of the O sp orbital, indicating a strong interaction between O, Ni, and Au. Similarly, by comparing the DOS of Pd-Au, Pt-Au and Rh-Au trimers before and after oxygen adsorption, it can be seen that the DOS just above the Fermi level basically do not change. However, for DOS just below the Fermi level, the contributions of Au sp and d and TM d orbitals are obviously weakened. The decreasing part mainly corresponds to the contribution of the O sp orbital, indicating a strong interaction between O, Au, and TM.

3.4 Bader charge analysis on O_2 molecule adsorption

To better analyze the charge transfer of the TM-Au(111)(TM=Ni, Rh, Pd, Pt) bimetallic surface after adsorbing oxygen molecules, we conducted a Bader charge analysis, as shown in Table 2. The oxygen atom forms a bond with the transition metal doped on the surface, and electrons are mainly transferred from the transition metal atom to the oxygen molecule. Among the four different metal-doped catalysts, Ni_{single}-Au(111), Rh_{single}-Au(111), Pd_{single}-Au(111) and Pt_{single}-Au(111), the number of electrons lost by TM is 0.54, 0.37, 0.28 and 0.16 e, respectively. The number of electrons obtained by the O_2 molecule is -0.68, -0.48, -0.53 and -0.57 e, respectively. Among the four bimetallic catalyst surfaces of dimer structural units, Ni_{dimer}-Au(111), Rh_{dimer}-Au(111), Pd_{dimer}-Au(111) and Pt_{dimer}-Au(111), the number of electrons lost by TM is 0.51, 0.35, 0.26 and 0.15 e, respectively. However, the number of electrons obtained by the O_2 molecule is -0.77, -0.52, -0.46 and -0.52 e, respectively. Among the four bimetallic catalyst surfaces of the trimer structural units, Ni_{trimer}-Au(111), Rh_{trimer}-Au(111), Pd_{trimer}-Au(111) and Pt_{trimer}-Au(111), the number of electrons lost by TM is 0.47, 0.28, 0.23 and 0.11 e, and the number of electrons obtained by the O_2 molecule is -0.80, -0.53, -0.59 and -0.64 e, respectively.

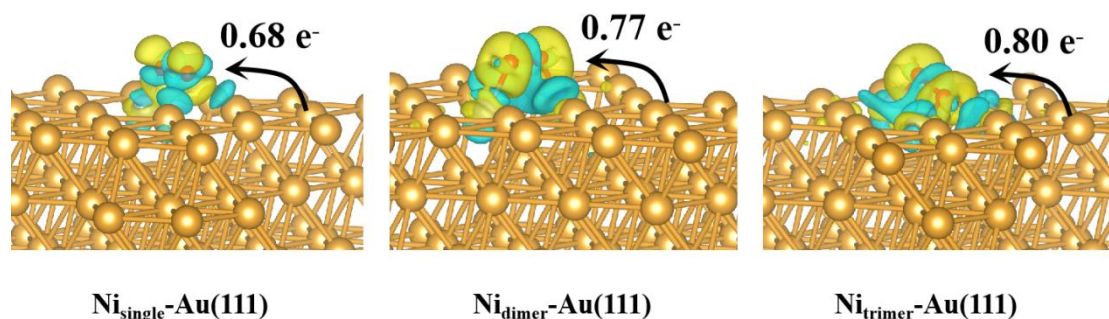


Figure 7. Differential charge density diagram of the stable configuration of O_2 molecules adsorbed on the surface of different structural units of Ni-Au(111) bimetal (green means losing electrons, yellow means gaining electrons)

Analyzing the above Bader charge data, it can be concluded that when TM=Ni, the number of charge transfers between the O_2 molecule and the bimetallic surface is the largest. To more intuitively observe the charge distribution of the Ni-Au(111) bimetallic surface after O_2 molecules are adsorbed,

this paper analyzes the differential charge density of the structures of Ni_{single}-Au(111), Ni_{dimer}-Au(111), and Ni_{trimer}-Au(111) after O₂ adsorption.

Combined with Table 2 and Figure 7, it can be seen that the change in bond length between O-O is consistent with the change in charge transfer number between O₂ and the bimetallic surface. The more charge an O₂ molecule receives from the surface, the longer the O-O bond becomes. When Ni is doped on the Au(111) surface in the form of a trimer, the number of charge transfers between O₂ molecules and the bimetal surface is the largest. The O₂ molecules obtain a charge of 0.80e from the surface. At the same time, the length of the bond between O-O in the adsorbed configuration also stretched to the maximum, which is 1.455 Å. The more electrons oxygen molecules gain from the surface, the stronger the interaction with the surface, which leads to weakening of the forces between oxygen atoms.

4. CONCLUSIONS

In this work, DFT calculations were used to study the adsorption of O₂ molecules on TM-Au(111)(TM=Ni, Rh, Pd, Pt) surfaces doped with different structural units, such as single atoms, dimers, and trimers. First, four different transition metals were doped with different structural units on the Au(111) surface to obtain a gold-based bimetallic catalyst. Then, O₂ molecules were adsorbed on the surface of these 12 gold-based bimetallic catalysts, and various structures were investigated to achieve a stable configuration. The adsorption configuration was analyzed from the adsorption energy, the bond length between O-O, state density analysis, and Bader charge transfer. It was concluded that after these four doped metals were doped on the Au surface with a monomer structure, their adsorption and activation of O₂ were poor. The stability of the trimeric structural unit doped with O₂ was less than that of the dimer, but the bond length of oxygen and the number of charge transfer were larger than those of the dimer. When TM=Ni, the stability, O-O bond length and number of charge transfer after oxygen adsorption were greater than those of other metals with the same structure. When Ni was doped in the form of a trimer to obtain a Ni_{trimer}-Au(111) bimetallic surface, its adsorption energy after adsorbing oxygen was -180.43 kJ/mol, the bond length between O-O was 1.455 Å, and the O₂ molecule obtained 0.80 e electrons from the surface. Therefore, the Ni-Au bimetallic catalyst doped on the surface of Au(111) in an aggregated state had a better effect on the adsorption and activation of oxygen. This research will have a particular reference value for the design of gold-based bimetallic catalysts and the study of their catalytic mechanism in reactions involving oxygen.

ACKNOWLEDGMENTS

We gratefully acknowledge financial support from National Natural Science Foundation of China (Grant no. 21571119)

References

1. M. Sankar, N. Dimitratos, P. J. Miedziak, P. P. Wells, C. J. Kiely, G. J. Hutchings, *Chem. Soc. Rev.*, 41(2012)8099–8139.
2. G. Sormojai, *Introduction to surface chemistry and catalysis*. John Wiley & Sons, 1994.

3. W. Chen, W. Schneider, C. Wolverton, *J. Phys. Chem. C*, 118 (2014)8342–8349.
4. J. K. Norskov, T. Bligaard, J. Rossmeisl, C. H. Christensen, *Nat. Chem.*, 11(2009)37–46.
5. J. Gu, Y. W. Zhang, F. Tao, *Chem. Soc. Rev.*, 41(2012)8050–8065.
6. J. Lin, Q. B. Liu, X. Zhang, *Angew. Chem. Int. Ed.*, 51(2012)2920–2924.
7. W. Yu, M. D. Porosoff, J. G. Chen, *Chem. Soc. Rev.*, 112(2012)5780–5817.
8. F. Tao, *Chem. Soc. Rev.*, 41(2012)77977–7979.
9. Y. Fan, J. Zhang, Y. Qiu, J. Zhu, Y. Zhang, G. Hu, *Comput. Mater. Sci.*, 138(2017)255–266.
10. K. D. Gilroy, A. Rnditskiy, H. C. Peng, D. Qin Y. Xia, *Chem. Rev.*, 116(2016)10414–10472.
11. M. Zong, Z. Ding, W. He, J. Luo, Z. Tang, *Int. J. Electrochem. Sci.*, 15(2020)2634–2647.
12. M. Haruta, *Chem. Lett.*, 1987,405–408.
13. M. Haruta, S. Tsubota, T. Kobayashi, H. Kageyama, M. J. Genet, B. Delmon, *J. Catal.*, 144(1993)175–192.
14. J. Luo, Y. Liu, L. Zhang, C. Liang, *ACS Appl. Mater. Interfaces.*, 11(2019)35468–35478.
15. D. Enache, J. Edwards, P. Landon, B. Solsona-Espriu, A. Carley, A. Herzing, M. Watanabe, C. Kiely, D. Knight, G. Hutchings, *Science* 311(2006)362–365.
16. H. Li, G. Henkelman, *J. Phys. Chem. C*, 121(2017)27504–27510.
17. W. Yi, W. Yuan, Y. Meng, S. Zou, Y. Zhou, W. Hong, J. Che, M. Hao, B. Ye, L. Xiao, Y. Wang, H. Kobayashi, J. Fan, *ACS Appl. Mater. Interfaces*, 9(2017)31853–31860.
18. Y. Nanba, M. Koyama. *J. Phys. Chem. C.*, 123(2019)28114–28122.
19. W. Y. Yu, G. M. Mullen, C. B. Mullins, *J. Phys. Chem. C.*, 117(2013)19535–19543.
20. M. Grabau, H. P. Steinrück, C. Papp, *Surf. Sci.*, 677(2018)254–257.
21. M. G. Sensoy, M. M. Montemore, *J. Phys. Chem. C*, 124(2020)8843–8853.
22. H. Farrokhpour, M. Ghandehari, K. Eskandari, *Appl. Surf. Sci.*, 457(2018)712–725.
- A. Kandory, R. Yahiaoui, E. Herth, H. Cattley, T. Gharbi, G. Herlem, *Int. J. Electrochem. Sci.*, 11(2016)7540–7552.
23. G. Chen, K. Kuttiyiel, D. Su, M. Li, C. H. Wang, D. Buceta, C. Du, Y. Gao, G. Yin, K. Sasaki, *Chem. Mater.*, 28(2016)5274–5281.
- A. Beniya, Y. Ikuta, N. Isomura, H. Hirata, Y. Watanabe, *ACS Catal.*, 7(2017)1369–1377.
24. W. Zhong, Y. Liu, D. Zhang, *J. Phys. Chem. C*, 116(2012)2994–3000.
25. T. Liu, M. Liu, Y. P. Li, Z. Y. Yu, *Int. J. Electrochem. Sci.*, 11(2016)685–691.
26. R. N. Singh, R. Awasthi, C. S. Sharma, *Int. J. Electrochem. Sci.*, 9(2014)5607–5639.
27. M. M. Montemore, M. A. Spronsen, R. J. Madix, C. M. Friend, *Chem. Rev.*, 118(2018)2816–2882.
28. D. Qu, Y. Tao, L. Guo, Z. Xie, W. Tu and H. Tang, *Int. J. Electrochem. Sci.*, 10(2015)3363–3371.
29. S. Chao, Z. Lu, Z. Bai, Q. Cui, J. Qiao, Z. Yang, L. Yang, *Int. J. Electrochem. Sci.*, 8(2013)8786–8799.
30. T. Duan, R. Zhang, L. Ling, B. Wang, *J. Phys. Chem. C*, 120(2016)2234–2246.
31. Y. Sha, T. H. Yu, B. V. Merinov, W. A. Goddard. *ACS Catal.*, 4(2014)1189–1197.
32. G. Rostamikia, R. J. Patel, I. Merino-Jimenez, M. Hickner, M. J. Janik, *J. Phys. Chem. C*, 121(2017)2872–2881.
33. M. Ma, H. A. Hansen, M. Valenti, Z. Wang, A. Cao, M. Dong, W. A. Smith, *Nano Energy*, 42(2017)51–57.
34. H. Y. Kim, G. Henkelman, *ACS Catal.*, 3(2013)2541–2546.
35. H. Wang, T. Shen, S. Duan, Z. Chen, X. Xu, *ACS Catal.*, 9(2019)11116–11124.
- A. Hussain, *J. Phys. Chem. C*, 117(2013)5084–5094.
36. W. Y. Yu, L. Zhang, G. M. Mullen, *J. Phys. Chem. C*, 119(2015)11754–11762.
37. N. M. Wilson, Y. T. Pan, Y. T. Shao, J. M. Zuo, D. W. Flaherty, *ACS Catal.*, 8(2018)2880–2889.
38. M. Smiljanić, Z. Rakočević, S. Štrbac, *Int. J. Electrochem. Sci.*, 8(2013)4941–4954.
39. Y. Guan, E. J. M. Hensen, *J. Catal.*, 305(2013)135–145.
40. M. G. Sensoy, M. M. Montemore, *J. Phys. Chem. C*, 124(2020)8843–8853.
41. S. Han, C. B. Mullim, *ACS Catal.*, 8(2018)3641–3649.

42. Y. F. Han, Z. Zhong, K. Ramesh, L. Chen, T. White, Q. Tay, S. N. Yaakub, Z. Wang, *J. Phys. Chem. C*, 111(2007)8410–413.
43. Y. Wang, P. B. Balbuena, *J. Phys. Chem. B*, 108(2004)4376–4384.
44. Y. Xu, A. V. Ruban, M. Mavrikakis, *J. Am. Chem. Soc.*, 126(2004)4717–4725.
45. L. M. C. Pinto, G. Maia, *J. Phys. Chem. C*, 119(2015)8213–8216.
46. C. R. Chang, B. Long, X. F. Yang, J. Li, *J. Phys. Chem. C*, 119(2015)16072–16081.
47. J. Baltrusaitis, M. Valter, A. Hellman, *J. Phys. Chem. C*, 120(2016)1749–1757.
48. Q. Wang, D. Tichit, F. Meunier, H. Guesmi, *J. Phys. Chem. C*, 124(2020)9979–9989.
49. X. Jia, W. An, *J. Phys. Chem. C*, 122(2018)21897–21909.
50. H. Li, E. J. E. Jr, C. B. Mullins, H. Graeme, *J. Phys. Chem. C*, 122(2018)22024–22032.
51. M. Xue, J. F. Jia, H. S. Wu, *Comput. Theor. Chem.*, (2021), doi: <https://doi.org/10.1016/j.comptc.2021.113439>
52. H. C. Ham, G. S. Hwang, J. Han, S. W. Nam, T. H. Lim, *J. Phys. Chem. C*, 113(2009)12943–12945.
53. J. S. Jirkovský, I. Panas, E. Ahlberg, M. Halasa, S. Romani, D. J. Schiffrin, *J. Am. Chem. Soc.*, 133(2011)19432–19441.
54. H. Guesmi, C. Louis, L. Delannoy, *Chem. Phys. Lett.*, 503(2011)97–100.
55. F. R. Lucci, L. Zhang, T. Thuening, M. B. Uhlman, A. C. Schilling, G. Henkelman, E. H. Sykes, *Surf. Sci.*, 677(2018)296–300.
56. C. R. Chang, X. F. Yang, B. Long, J. Li, *ACS Catal.*, 3(2013)1693–1699.
57. J. Gong, C. B. Mullins, *Acc. Chem. Res.*, 42(2009)1063–1073.
58. M. Eagleson, *Concise Encyclopedia of Chemistry*, Walter de Gruyter: Berlin, 1994.

© 2022 The Authors. Published by ESG (www.electrochemsci.org). This article is an open access article distributed under the terms and conditions of the Creative Commons Attribution license (<http://creativecommons.org/licenses/by/4.0/>).